

Supporting Information

Transparent and flexible high-power supercapacitor based on carbon nanotube fibre aerogels

*Evgeny Senokos^{1,2}, Moumita Rana¹, Maria Vila¹, Julio Fernández-Cestau¹, Rubén D. Costa¹,
Rebeca Marcilla^{2*}, Juan Jose Vilatela^{1*}*

1) IMDEA Materials Institute, C/ Eric Kandel, 2, Getafe, 28906, Madrid, Spain

2) Electrochemical Processes Unit, IMDEA Energy, Avda. Ramón de la Sagra, 3, 28937
Móstoles, Madrid, Spain

* rebeca.marcilla@imdea.org, juanjose.vilatela@imdea.org

Experimental part

Materials

Thiophene (extra purity $\geq 99\%$) and ferrocene (purity = 98%) obtained from Acros Organics and 2-butanol (purity $>99\%$) from Sigma Aldrich were used for synthesis of CNT fibres. Ferrocene was purified by a sublimation/recrystallization process. N-methyl-N-butylpyrrolidinium bis(trifluoromethanesulfonyl)imide, Pyr₁₄TFSI ionic liquid (high purity, $>99.5\%$) was received from Solvionic and stored in the glove box. Poly(vinylidene fluoride-co-

hexafluoropropylene) (PVDF-co-HFP) (average $M_w \sim 400,000$, average $M_n \sim 130,000$, pellets) was purchased from Sigma Aldrich and utilized as polymer matrix for polymer electrolyte.

Synthesis of CNT fibres

CNTs synthesized by floating catalyst CVD method at 1250 °C in controlled hydrogen atmosphere were continuously spun from a vertical reactor in the shape of fibres as discussed elsewhere.[1] The precursor feed rate was 2 ml/h while winding rate was fixed at 3 m/min. The fibres were spun on aluminum foil substrate for assembling symmetric all-solid SCs in Swagelok cell and on both sides of PE membrane to fabricate transparent free-standing SC device. The mass of single layer CNT fibre electrodes was estimated based on linear density of the material. For this purpose, CNT fibres were spun at identical conditions for 5 minutes and accurately weighted using microbalance. The total length of spun material was calculated from the spinning rate. The procedure was repeated three times in order to evaluate an error of the mass measurement.

Fabrication of all-solid SC devices

Prior to assembling SC devices the electrodes of CNT fibres deposited on aluminum foil were cut to a coin-like shape with a projected surface area of 0.785 cm². The coin shaped devices were prepared by sandwiching a PE membrane between two bare CNT fibre electrodes and pressing the structure in 2-electrode Swagelok cell. PE membrane was produced by casting and doctor blading the solution containing 60 wt.% of Pyr₁₄TFSI ionic liquid and 40 wt.% of PVDF-co-HFP. The details of the preparation procedure has been previously discussed.[2]

Fabrication of free-standing transparent SCs based on single layer CNT fibre electrodes consisted of direct spinning of thin CNT films on both sides of PE membrane supported on a rotating drum. The composite devices was then inserted in a transparent plastic pouch film, applying a moderate pressure during 10 min and laminating the device using a conventional

pouch laminator. Multiple layers of CNT fibre aerogel could be deposited by controlling the number of turns of the rotating drum.

Materials characterization

Morphology of single layer CNT fibres was analyzed by scanning electron microscopy (SEM). SEM images were acquired using a dual beam FIB-FEGSEM microscope (Helios NanoLab 600i FEI) at acceleration voltage of 5 kV. The structure of produced CNT fibres was also studied by transmission electron microscopy (TEM). The images were recorded with a Talos F200X microscope (FEI), operating at 80-200 kV. TEM samples were prepared by dispersing a small amount of CNT fibres in absolute ethanol and sonicating it in an ultrasonic power bath for 30 minutes. After that, the dispersion was drop cast onto a copper TEM grid.

General information about the composition and structure of the CNT fibre aerogels can be found in references [31]–[33].

Optical transmittance spectra were acquired using a double beam Shimadzu UV-2600 ultraviolet-visible spectrophotometer. All spectra were obtained in the wavelength range 350-1000 nm with wavelength resolution of 0.95 nm and wavelength accuracy of 0.5 nm. Each experimental spectrum was corrected by subtracting the background spectrum of air.

Sheet resistance of CNT fibre films was measured using the four-probe technique on a KEITHLEY 2450 Source Meter. A nonconductive glass with four equidistant and rectangular spaced gold sputtered contacts was used as a substrate for CNT fibres films. The samples with different number of CNT fibre layers were produced consecutively on the same date to avoid discrepancy between samples. Sheet resistance (R_s) was estimated for a square area between two gold contacts with a length and width of 1 cm. Correspondingly, the R_s values directly obtained from the measurement were expressed in ohms per square (Ω/sq).

Electrochemical measurements

All-solid symmetric EDLCs were characterized by galvanostatic charge-discharge (CD) and electrochemical impedance spectroscopy (EIS). CD tests were performed from 0 to 3.5V at current densities from 1 to 10 mA cm⁻². Specific capacitance of full devices (C_{cell}) was calculated from the slope of the discharge curve as $C_{cell} = I/\text{slope}$. The slope values are estimated from linear region of discharge profile discarding the first segment at the beginning of the discharge curve, where $R^2 > 0.98$. In symmetric devices the specific capacitance of a single electrode (C_s) was extracted as $C_s = 4C_{cell}$. All reported capacitance values measured in full cell correspond to C_s . Values of Equivalent Series Resistance (ESR), real energy (E_{real}) and power (P_{real}) densities were calculated from discharge curves of EDLCs devices according to the following equations:

$$E_{real} = I \int V dt, \quad (1)$$

$$P_{real} = \frac{E_{real}}{t_{dis}}, \quad (2)$$

$$ESR = \Delta V / 2I, \quad (3)$$

where I is the constant current applied, t_{dis} is the discharge time and ΔV is the ohmic drop observed at the beginning of the discharge curve. Cycle stability tests of free-standing transparent SC devices was carried out over 20,000 CD cycles from 0V to 3.5V at 5 mA cm⁻². EIS of all-solid SCs were obtained in the frequency range from 200 kHz to 10 mHz at a bias voltage of 0V with a potential amplitude of 10 mV. For measurements on single CNT fibre electrodes deposited on aluminum (Al) current collector and tested in a Swagelok cell, it was confirmed that the Al current collectors gave a negligible contribution to capacitance measurements, particularly at high currents.

Supplementary Figures and Tables

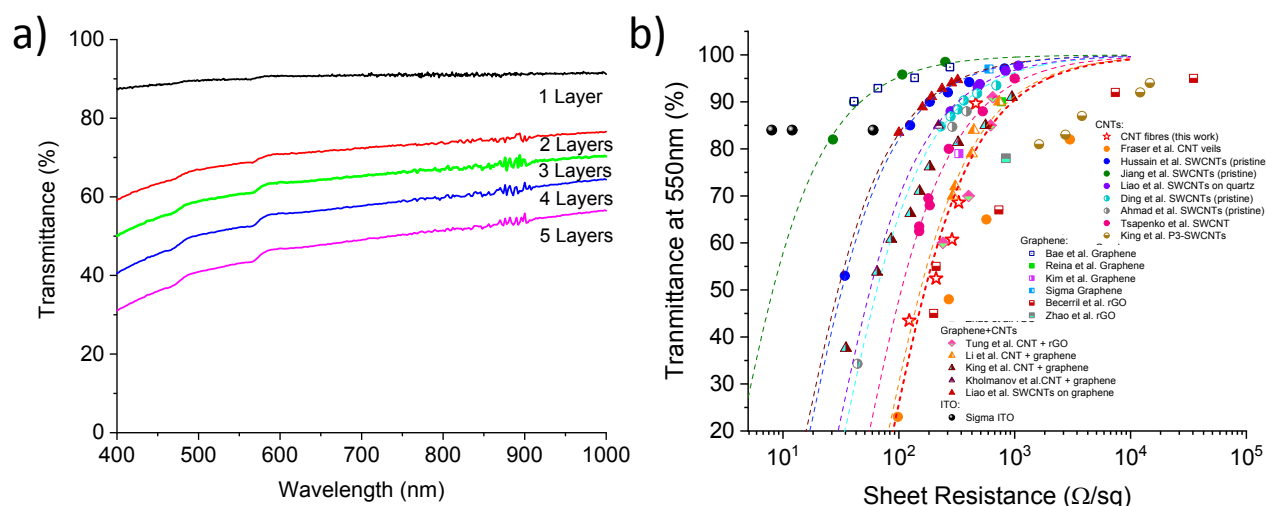


Figure 1S. a) Optical transmittance spectra of 1, 2, 3, 4 and 5 layers of CNT fibres, and b) a plot of transmittance at 550nm as a function of sheet resistance comparing optoelectronic properties of CNT fibres to the performance of reported transparent conductors based on pristine carbon materials.[3]–[22] Dashed lines are obtained by fitting the data using Equation 1. Detailed values are included in Table S1 (Supporting Information).

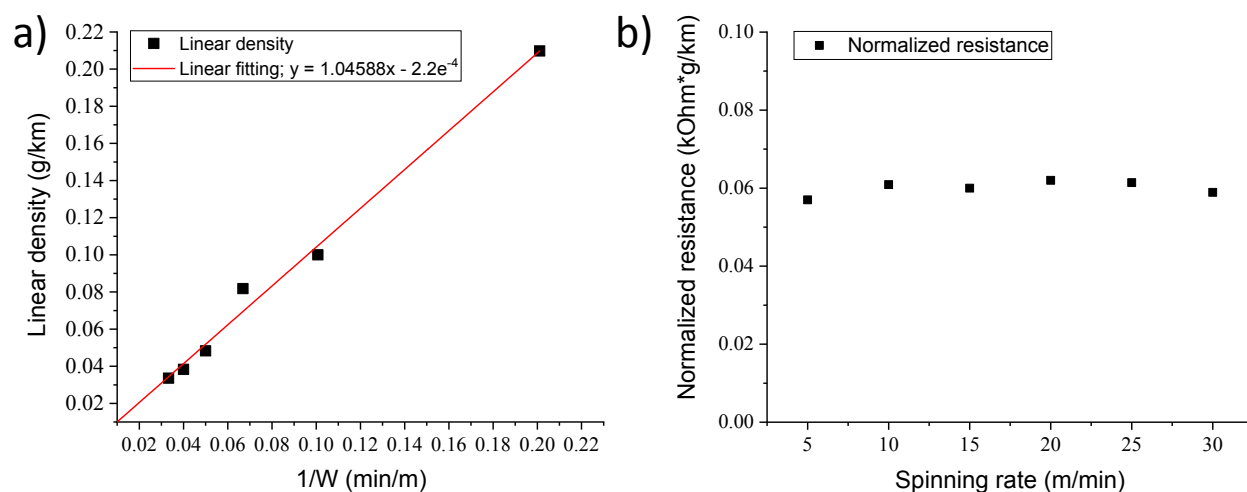


Figure 2S. Effect of some processing parameters on areal density. a) Fibre linear density scales with the reciprocal of spinning rate. b) A plot of sheet resistance versus fibre spinning rate shows a linear dependence.

In the context of CNT fibres spun from the gas phase, fibre linear density (i.e. mass per unit length, ρ_l) can be very accurately measured by weighing a known length of fibre. This makes it a very useful metric for normalization.

Increasing winding rate increases the draw ratio applied to the CNT aerogel. Drawing has the expected effect of thinning down the incoming CNT aerogel but without altering the CVD reaction. CNT fibre linear density scales with the reciprocal of spinning rate (s) (Figure 2Sa). A plot of R_s against s shows a linear dependence, which implies that the effect of varying the spinning rate is simply changing the areal density of the CNT network. Under these conditions, sheet resistance can be related to spinning parameters by

$$R_s = \frac{\rho_v \times s \times w}{\sigma_{DC} \times m/t} \quad (4)$$

Where ρ_v is the volumetric density, m/t the rate of CNT fibre mass produced in the reaction per unit time and s the width of the transparent conductor. Since m/t is fixed under a set of synthesis

conditions, the linear dependence with s implies that $\frac{\rho_v \times w}{\sigma_{DC}}$ is a constant.

Similarly, Fraser et al have shown that changing carrier gas flow rate in the reaction is another method to modify areal density, and demonstrated that it scales linearly with fibre linear density and transparency.[6] Effectively, they fixed s and varied w .

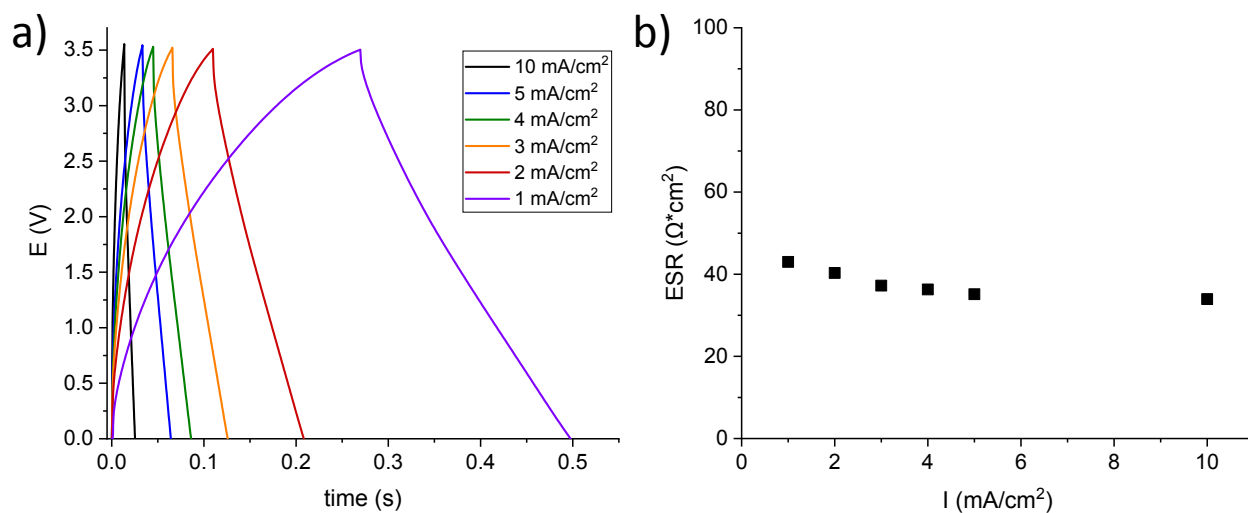


Figure 3S. a) CD curves at different current densities obtained for EDLC devices with single filament CNT fibre electrodes (i.e. $3.5 \mu\text{g cm}^{-2}$ for two electrodes, transparent) assembled and tested in Swagelok cell, and b) equivalent series resistance (ESR) extracted from the ohmic drop of CD curves measured at different current densities.

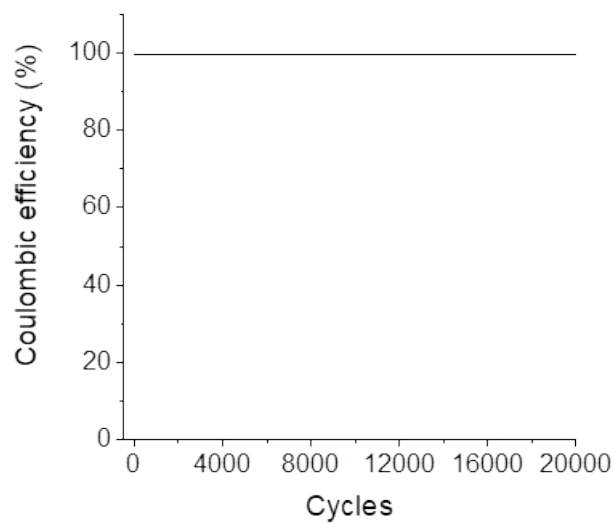


Figure 4S. Coulombic efficiency of the transparent free-standing single filament EDLC during CD test over 20,000 cycles at 5 mA cm^{-2} and operating voltage of 3.5V.

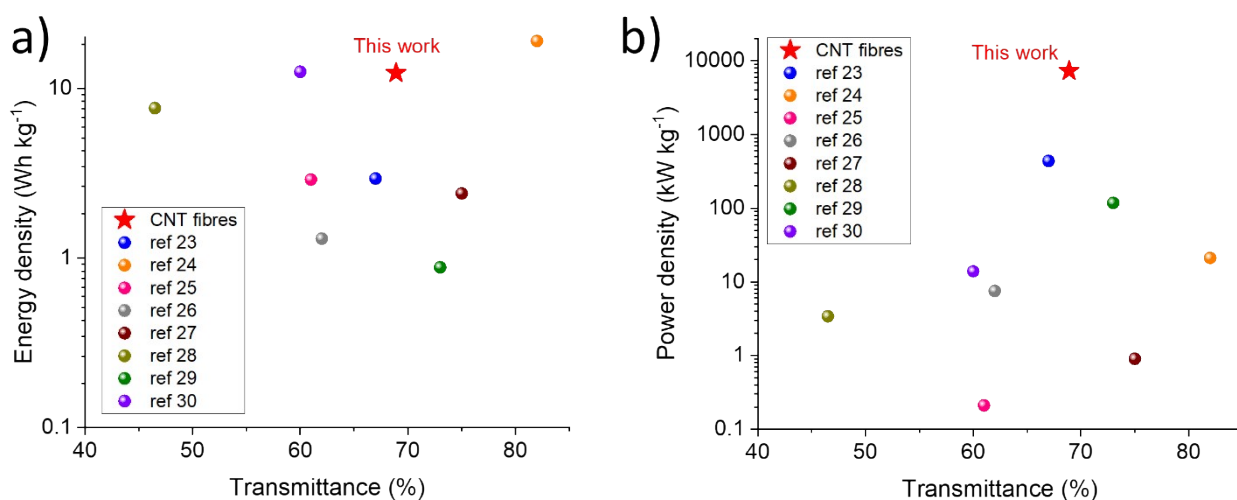


Figure 5S. The plots of a) energy density and b) power density against optical transmittance at 550 nm for full-cell transparent supercapacitors presented in this work and reported in literature.[23]–[30]

Table S1. Sheet resistance and optical transmittance for different carbon-based transparent conductors reported in literature.

Material	Sheet resistance, ohm/sq	Transmittance, %
CNT fibres (this work)	462	89.7
	329	68.6
	288	60.7
	210	52.4
	123	43.5
SWCNT[15]	150	62.5
	150	63.5
	185	68
	180	69.5
	270	80
	530	88
P3-SWCNT[19]	1623	81
	2739	83
	3814	87
	12130	92
	14706	94
	236000	97
rGO[8]	35000	95
	7400	92
	730	67
	210	55
	200	45
rGO[3]	840	78
graphene[20]	330	79
graphene[14]	770	90
graphene[9]	276	97.4
	137	95.1
	66	92.9
	41	90.1
graphene[13]	600	97

ITO[12]	8 12	84 84
ITO[11]	60	84
CNT+rGO[4]	647 620 400 240	91 85 70 60
CNT+graphene[17]	735 444 427 307 292	90 84 79 72 70
CNT+graphene[18]	947 560 325 185 151 126 86 65 35	91 85 81 76 71 66 61 54 37
CNT+graphene[21]	220	85
CNT veils film[6]	3000 570 270 98	82 65 48 23
SWCNTs (pristine)[5]	817 405 265 185 125 34.2	97.1 94.2 92 90 85 53
SWCNTs (pristine)[22]	252 107 41 27	98.5 95.8 90 82
SWCNTs on quartz[16]	1078 834 500 480 280	97.7 96.6 93.8 93.2 88
SWCNTs on graphene[16]	322 286 236 192 160 100	94.7 94 92.8 91.1 88.9 83.5
SWCNTs (pristine)[7]	695 475 365 324 280 230	93.5 91.8 90.3 88.4 86.9 84.8
SWCNTs (pristine)[10]	385 290 44	88 84.7 34.3

Table S2. Comparison of transparent and flexible SCs.

Electrode material	Electrolyte	Maximum energy density, Wh kg ⁻¹	Maximum power density, kW kg ⁻¹	Transparency, %
CNT fibres (this work)	Py ₁₄ TFSI/PVDF-co-HFP	12.3	7290	68.9
Graphene[23]	H ₃ PO ₄ -PVA	2.94	438.6	67
rGO[25]	H ₃ PO ₄ -PVA	2.9	0.21	61
Graphene[29]	H ₂ SO ₄ -PVA	0.88	118	73
SWCNTs[24]	TBAPF ₆ -PMMA/PC-ACN	19	21.1	82
SWCNTs[30]	LiClO ₄ -EC/DEC/DMC (liquid)	12.5	13.9	60
CNTs+In ₂ O ₃ [26]	LiClO ₄ -EC/DEC/DMC (liquid)	1.3	7.5	62
CNT[27]	H ₃ PO ₄ -PVA	2.4	0.9	75
Graphene[28]	H ₂ SO ₄ -PVA	7.64	3.4	46.5

REFERENCES

- [1] V. Reguero, B. Alemán, B. Mas, and J. J. Vilatela, Controlling Carbon Nanotube Type in Macroscopic Fibers Synthesized by the Direct Spinning Process, *Chemistry of Materials*, **26**, 11, 2014, pp. 3550–3557.
- [2] E. Senokos, V. Reguero, L. Cabana, J. Palma, R. Marcilla, and J. J. Vilatela, Large-Area, All-Solid, and Flexible Electric Double Layer Capacitors Based on CNT Fiber Electrodes and Polymer Electrolytes, *Advanced Materials Technologies*, **2**, 7, 2017, p. 1600290.
- [3] J. Zhao, S. Pei, W. Ren, L. Gao, and H.-M. Cheng, Efficient preparation of large-area graphene oxide sheets for transparent conductive films, *ACS nano*, **4**, 9, 2010, pp. 5245–5252.
- [4] V. C. Tung *et al.*, Low-temperature solution processing of graphene– carbon nanotube hybrid materials for high-performance transparent conductors, *Nano letters*, **9**, 5, 2009, pp. 1949–1955.
- [5] A. Hussain *et al.*, Floating catalyst CVD synthesis of single walled carbon nanotubes from ethylene for high performance transparent electrodes, *Nanoscale*, **10**, 20, 2018, pp. 9752–9759.
- [6] I. S. Fraser, M. S. Motta, R. K. Schmidt, and A. H. Windle, Continuous production of flexible carbon nanotube-based transparent conductive films. *Science and technology of advanced materials*, **11**, 4, 2010, p. 045004.

- [7] E.-X. Ding, Q. Zhang, N. Wei, A. T. Khan, and E. I. Kauppinen, High-performance single-walled carbon nanotube transparent conducting film fabricated by using low feeding rate of ethanol solution, *Royal Society open science*, **5**, 6, 2018, p. 180392.
- [8] H. A. Becerril, J. Mao, Z. Liu, R. M. Stoltenberg, Z. Bao, and Y. Chen, Evaluation of solution-processed reduced graphene oxide films as transparent conductors, *ACS nano*, **2**, 3, 2008, pp. 463–470.
- [9] S. Bae *et al.*, Roll-to-roll production of 30-inch graphene films for transparent electrodes, *Nature nanotechnology*, **5**, 8, 2010, p. 574.
- [10] S. Ahmad *et al.*, Roles of sulfur in floating-catalyst CVD growth of single-walled carbon nanotubes for transparent conductive film applications, *Chemical Engineering Journal*, **378**, 2019, p. 122010.
- [11] Indium tin oxide coated glass slide (703184) from Sigma Aldrich, <https://www.sigmaaldrich.com/catalog/product/ALDRICH/703184?lang=en®ion=GB>, [accessed 01.05.2020].
- [12] Indium tin oxide coated glass slide (703192) from Sigma Aldrich, <https://www.sigmaaldrich.com/catalog/product/ALDRICH/703192?lang=en®ion=GB>, [accessed 01.05.2020].
- [13] Monolayer graphene film (773719) from Sigma Aldrich, <https://www.sigmaaldrich.com/catalog/product/ALDRICH/773719?lang=en®ion=GB>, [accessed 01.05.2020].
- [14] A. Reina *et al.*, Large area, few-layer graphene films on arbitrary substrates by chemical vapor deposition, *Nano letters*, **9**, 1, 2009, pp. 30–35.
- [15] A. P. Tsapenko *et al.*, Highly conductive and transparent films of HAuCl₄-doped single-walled carbon nanotubes for flexible applications, *Carbon*, **130**, 2018, pp. 448–457.
- [16] Y. Liao *et al.*, Enhanced Tunneling in a Hybrid of Single-Walled Carbon Nanotubes and Graphene, *ACS Nano*, **13**, 10, 2019, pp. 11522–11529.
- [17] C. Li *et al.*, Graphene nano-“patches” on a carbon nanotube network for highly transparent/conductive thin film applications, *The Journal of Physical Chemistry C*, **114**, 33, 2010, pp. 14008–14012.
- [18] P. J. King, U. Khan, M. Lotya, S. De, and J. N. Coleman, Improvement of transparent conducting nanotube films by addition of small quantities of graphene, *Acs Nano*, **4**, 7, 2010, pp. 4238–4246.
- [19] P. J. King, T. M. Higgins, S. De, N. Nicoloso, and J. N. Coleman, Percolation Effects in Supercapacitors with Thin, Transparent Carbon Nanotube Electrodes, *ACS Nano*, **6**, 2, 2012, pp. 1732–1741.
- [20] K. S. Kim *et al.*, Large-scale pattern growth of graphene films for stretchable transparent electrodes, *nature*, **457**, 7230, 2009, p. 706.
- [21] I. N. Kholmanov *et al.*, Optical, electrical, and electromechanical properties of hybrid graphene/carbon nanotube films, *Advanced Materials*, **27**, 19, 2015, pp. 3053–3059.

- [22] S. Jiang *et al.*, Ultrahigh-performance transparent conductive films of carbon-welded isolated single-wall carbon nanotubes, *Science advances*, **4**, 5, 2018, p. eaap9264.
- [23] Y. Gao *et al.*, Transparent, flexible, and solid-state supercapacitors based on graphene electrodes, *APL materials*, **1**, 1, 2013, p. 12101.
- [24] R. Yuksel, Z. Sarioba, A. Cirpan, P. Hiralal, and H. E. Unalan, Transparent and flexible supercapacitors with single walled carbon nanotube thin film electrodes, *ACS applied materials & interfaces*, **6**, 17, 2014, pp. 15434–15439.
- [25] T. Aytug *et al.*, Vacuum-assisted low-temperature synthesis of reduced graphene oxide thin-film electrodes for high-performance transparent and flexible all-solid-state supercapacitors, *ACS applied materials & interfaces*, **10**, 13, 2018, pp. 11008–11017.
- [26] P.-C. Chen, G. Shen, S. Sukcharoenchoke, and C. Zhou, Flexible and transparent supercapacitor based on In₂O₃ nanowire/carbon nanotube heterogeneous films, *Applied Physics Letters*, **94**, 4, 2009, p. 43113.
- [27] T. Chen, H. Peng, M. Durstock, and L. Dai, High-performance transparent and stretchable all-solid supercapacitors based on highly aligned carbon nanotube sheets, *Scientific reports*, **4**, 2014, p. 3612.
- [28] N. Li *et al.*, Free-standing and transparent graphene membrane of polyhedron box-shaped basic building units directly grown using a nacl template for flexible transparent and stretchable solid-state supercapacitors, *Nano letters*, **15**, 5, 2015, pp. 3195–3203.
- [29] P. Xu *et al.*, Laminated ultrathin chemical vapor deposition graphene films based stretchable and transparent high-rate supercapacitor, *ACS nano*, **8**, 9, 2014, pp. 9437–9445.
- [30] Z. Niu *et al.*, A Repeated Halving Approach to Fabricate Ultrathin Single-Walled Carbon Nanotube Films for Transparent Supercapacitors, *Small*, **9**, 4, 2013, pp. 518–524.
- [31] C. Santos, E. Senokos, J. C. Fernández-Toribio, Á. Ridruejo, R. Marcilla, and J. J. Vilatela, Pore structure and electrochemical properties of CNT-based electrodes studied by: In situ small/wide angle X-ray scattering, *Journal of Materials Chemistry A*, **7**, 10, 2019, p. 5305-5314.
- [32] B. Alemán, M. Vila, and J. J. Vilatela, Surface Chemistry Analysis of Carbon Nanotube Fibers by X-Ray Photoelectron Spectroscopy, *physica status solidi (a)*, **215**, 19, 2018, p. 1800187.
- [33] B. Alemán and J. J. Vilatela, Chapter 6 - Multiscale Engineering of Carbon Nanotube Fibers, in *Micro and Nano Technologies*, M. J. Schulz, V. Shanov, Z. Yin, and M. B. T.-N. S. M., William Andrew Publishing, 2019, pp. 113–147.